

ADCN: An Anisotropic Density-Based Clustering Algorithm for Discovering Spatial Point Patterns with Noise

Abstract

Density-based clustering algorithms such as DBSCAN have been widely used for spatial knowledge discovery as they offer several key advantages compared to other clustering algorithms. They can discover clusters with arbitrary shapes, are robust to noise and do not require prior knowledge (or estimation) of the number of clusters. The idea of using a scan circle centered at each point with a search radius Eps to find at least $MinPts$ points as a criterion for deriving local density is easily understandable and sufficient for exploring isotropic spatial point patterns. However, there are many cases that cannot be adequately captured this way, particularly if they involve linear features or shapes with a continuously changing density such as a spiral. In such cases, DBSCAN tends to either create an increasing number of small clusters or add noise points into large clusters. Therefore, in this paper, we propose a novel anisotropic density-based clustering algorithm (ADCN). To motivate our work, we introduce synthetic and real-world cases that cannot be sufficiently handled by DBSCAN (and OPTICS). We then present our clustering algorithm and test it with a wide range of cases. We demonstrate that our algorithm can perform as equally well as DBSCAN in cases that do not explicitly benefit from an anisotropic perspective and that it outperforms DBSCAN in cases that do. Finally, we show that our approach has the same time complexity as DBSCAN and OPTICS, namely $O(n \log n)$ when using a spatial index and $O(n^2)$ otherwise. We provide an implementation and test the runtime over multiple cases.

Keywords: Anisotropic, clustering, noise, spatial point patterns

1 1. Introduction and Motivation

2 Cluster analysis is a key component of modern knowledge discovery, be it
3 as a technique for reducing dimensionality, identifying prototypes, cleansing
4 noise, determining core regions, or segmentation. A wide range of cluster-
5 ing algorithms, such as DBSCAN (Ester et al., 1996), OPTICS (Ankerst
6 et al., 1999), K-means (MacQueen et al., 1967), and Mean Shift (Comani-
7 ciu and Meer, 2002), have been proposed and implemented over the last
8 decades. Many clustering algorithms depend on *distance* as their main cri-
9 terion (Davies and Bouldin, 1979). They assume *isotropic* second-order ef-
10 fects (i.e., spatial dependence) among spatial objects thereby implying that
11 the magnitude of similarity and interaction between two objects mostly de-
12 pends on their distance. However, the genesis of many geographic phenomena
13 demonstrates clear *anisotropic* spatial processes. As for ecological and geo-
14 logical features, such as the spatial distribution of rocks (Hoek, 1964), soil
15 (Barden, 1963), and airborne pollution (Isaaks and Srivastava, 1989), their
16 spatial patterns vary in direction (Fortin et al., 2002). Similarly, data about
17 urban dynamics from social media, the census, transportation studies, and
18 so forth, are highly restricted and defined by the layout of urban spaces, and
19 thus show clear variance along directions. To give a concrete example, geo-
20 tagged images be it in the city or the great outdoors, show clear directional
21 patterns due to roads, hiking trails, or simply for the fact that they originate
22 from human, goal-directed trajectories. Isotropic clustering algorithms such
23 as DBSCAN have difficulties dealing with the resulting point patterns and ei-
24 ther fail to eliminate noise or do so at the expense of introducing many small
25 clusters. One such example is depicted in Figure 1. Due to the changing
26 density, algorithms such as DBSCAN will classify some noise, i.e., points be-
27 tween the spiral arms, as being part of the cluster. To address this problem,
28 we propose an anisotropic density-based clustering algorithm.

29 **More specifically, the research contributions of this paper are**
30 **as follows:**

- 31** • We introduce an anisotropic density-based clustering algorithm (ADCN
32 ¹). While the algorithm differs in the underlying assumptions, it uses

¹This paper is a substantially extended version of the short paper Mai et al. (2016). It also adds an open source implementation of ADCN, a test environment, as well as new evaluation results on a larger sample.

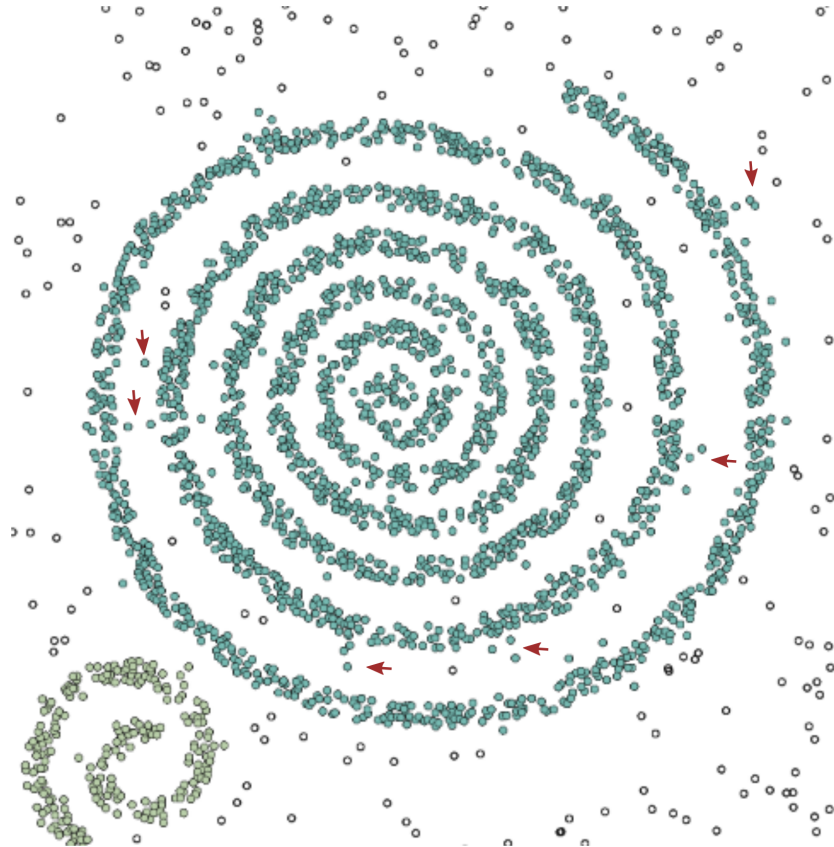


Figure 1: A spiral pattern clustered using DBSCAN. Some noise points are indicated by red arrows.

33 the same two parameters as DBSCAN, namely Eps and $MinPts$, thereby
 34 providing an intuitive explanation and integration into existing work-
 35 flows.

- 36 • We motivate the need for such algorithm by showing 12 synthetic and 8
 37 real-world use cases and each with 3 different noise definitions modeled
 38 as buffers that generate a total of 60 test cases.
- 39 • We demonstrate that ADCN performs as well as DBSCAN (and OPTICS) for isotropic cases but outperforms both algorithms in cases that
 40 benefit from an anisotropic perspective.
- 41 • We argue that ADCN has the same time complexity as DBSCAN and

43 OPTICS, namely $O(n \log n)$ when using a spatial index and $O(n^2)$
44 otherwise.

- 45 • We provide an implementation for ADCN and apply it to the use cases
46 to demonstrate the runtime behavior of our algorithm. As ADCN has
47 to compute whether a point is within an ellipse instead of merely relying
48 on the radius of the scan circle, its runtime is slower than DBSCAN
49 while remaining comparable to OPTICS. We discuss how the runtime
50 difference can be reduced by using a spatial index and by testing the
51 radius case first.

52 The remainder of the paper is structured as follows. First, in Section 2, we
53 discuss related work such as variants of DBSCAN. Next, we introduce ADCN
54 and discuss two potential realizations of measuring anisotropicity in Section
55 3. Use cases, the development of a test environment, and a performance
56 evaluation of ADCN are presented in Section 4. Finally, in Section 5, we
57 conclude our work and point to directions for future work.

58 **2. Related Work**

59 Clustering algorithms can be classified into several categories, including
60 but not limited to partitioning, hierarchical, density-based, graph-based, and
61 grid-based approaches (Han et al., 2011; Deng et al., 2011). Each of these cat-
62 egories contains several well known clustering algorithms with their specific
63 pros and cons. Here we focus on the density-based approaches.

64 Density-based clustering algorithms are widely used in big geo-data min-
65 ing and analysis tasks, like generating polygons from a set of points (Moreira
66 and Santos, 2007; Duckham et al., 2008; Zhong and Duckham, 2016), dis-
67 covering urban areas of interest (Hu et al., 2015), revealing vague cognitive
68 regions (Gao et al., 2017), detecting human mobility patterns (Huang and
69 Wong, 2015; Huang, 2017; Huang and Wong, 2016; Jurdak et al., 2015), and
70 identifying animal mobility patterns (Damiani et al., 2016).

71 Density-based clustering has many advantages over other approaches.
72 These advantages include: 1) the ability to discover clusters with arbitrary
73 shapes; 2) robustness to data noise; and 3) no requirement to pre-define the
74 number of clusters. While DBSCAN remains the most popular density-based
75 clustering method, many related algorithms have been proposed to compen-
76 sate some of its limitations. Most of them, such as OPTICS (Ankerst et al.,

77 1999) and VDBSCAN (Liu et al., 2007), address problems arising from den-
78 sity variations within clusters. Others, such as ST-DBSCAN (Birant and
79 Kut, 2007), add a temporal dimension. GDBSCAN (Sander et al., 1998)
80 extends DBSCAN to include non-spatial attributes into clustering and en-
81 ables the clustering of high dimensional data. NET-DBSCAN (Stefanakis,
82 2007) revises DBSCAN for network data. To improve the computational effi-
83 ciency, algorithms such as IDBSCAN (Borah and Bhattacharyya, 2004) and
84 KIDBSCAN (Tsai and Liu, 2006) have been proposed.

85 All of these algorithms use distance as the major clustering criterion.
86 They assume that the observed spatial patterns are isotropic, i.e., that in-
87 tensity dose not vary by direction. For example, DBSCAN uses a scan circle
88 with an Eps radius centered at each point to evaluate the local density around
89 the corresponding point. A cluster is created and expanded as long as the
90 number of points inside this circle (Eps -neighborhood) is larger than $MinPts$.
91 Consequently, DBSCAN does not consider the spatial distribution of the
92 Eps -neigborhood which poses problems for linear patterns.

93 Some clustering algorithms do consider local directions. However, most
94 of these so-call direction-based clustering techniques use spatial data which
95 have a pre-defined local direction, e.g., trajectory data. The *local direction*
96 of one point is pre-defined as the direction of the vector which is part of the
97 trajectories with the corresponding point as its origination or destination.
98 DEN (Zhou et al., 2010) is one direction-based clustering method which uses
99 a grid data structure to group trajectories by moving directions. PDC+
100 (Wang and Wang, 2012) is another trajectory specific DBSCAN variant that
101 includes the direction per point. DB-SMoT (Rocha et al., 2010) includes
102 both the direction and temporal information of GPS trajectories from fishing
103 vessel into the clustering process. Although all of these three direction-
104 based clustering algorithms incorporate local direction as one of the clustering
105 criteria, they can be applied to only trajectories data.

106 *Anisotropicity* (Fortin et al., 2002) describes the variation of directions
107 in spatial point processes in contrast to *isotropicity*. It is another way to
108 describe intensity variation in spatial point process other than first- and
109 second-order effects. *Anisotropicity* has been studied in the context of inter-
110 polation where a spatially continuous phenomenon is measured, such as di-
111 rectional variogram (Isaaks and Srivastava, 1989) and different modifications
112 of Kriging methods based on local anisotropicity (Stroet and Snepvangers,
113 2005; Machuca-Mory and Deutsch, 2013; Boisvert et al., 2009). In this pa-
114 per we focus on *anisotropicity* of spatial point processes. Researchers stud-

ied *anisotropicity* of spatial point processes from a theoretical perspective by analyzing their realizations such as detecting anisotropy in spatial point patterns (DErcole and Mateu, 2013) and estimating geometric anisotropic spatial point patterns (Rajala et al., 2016; Møller and Toftaker, 2014). Here, we study *anisotropicity* in the context of density-based clustering algorithms.

A few clustering algorithms take anisotropic processes into account. For instance, in order to obtain good results for crack detection, an anisotropic clustering algorithm (Zhao et al., 2015) has been proposed to revise DB-SCAN by changing the distance metric to geodesic distance. QUAC (Hanwell and Mirmehdi, 2014) demonstrates another anisotropic clustering algorithm which does not make an isotropic assumption. It takes the advantages of anisotropic Gaussian kernels to adapt to local data shapes and scales and prevents singularities from occurring by fitting the Gaussian mixture model (GMM). QUAC emphasizes the limitation of an isotropic assumption and highlights the power of anisotropic clustering. However, due to the use of anisotropic Gaussian kernels, QUAC can only detect clusters which have ellipsoid shapes. Each cluster derived from QUAC will have a major direction. In real-world cases, spatial pattern will show arbitrary shapes. Even more, the local direction is not necessary the same between and even within clusters. Instead, it is reasonable to assume that local direction can change continuously in different parts of the same cluster.

3. Introducing ADCN

In this section we introduce the proposed **Anisotropic Density-based Clustering with Noise** (ADCN).

3.1. Anisotropic Perspective on Local Density

Without predefined direction information from spatial datasets, one has to compute the *local direction* for each point based on the spatial distribution of points around it. The standard deviation ellipse (SDE) (Yuill, 1971) is a suitable method to get the major direction of a point set. In addition to the major direction (long axis), the flattening of the SDE implies how much the points are strictly distributed along the long axis. The flattening of an ellipse is calculated from its long axis a and short axis b as given by Equation 1:

$$f = \frac{a - b}{a} \quad (1)$$

¹⁴⁷ Given n points, the standard deviation ellipse constructs an ellipse to
¹⁴⁸ represent the orientation and arrangement of these points. The center of this
¹⁴⁹ ellipse $O(\bar{X}, \bar{Y})$ is defined as the geometric center of these n points and is
¹⁵⁰ calculated by Equation 2:

$$\bar{X} = \frac{\sum_{i=1}^n x_i}{n}, \bar{Y} = \frac{\sum_{i=1}^n y_i}{n} \quad (2)$$

¹⁵¹ The coordinates (x_i, y_i) of each point are normalized to the deviation from
¹⁵² the mean areal center point (Equation 3):

$$\tilde{x}_i = x_i - \bar{X}, \tilde{y}_i = y_i - \bar{Y}, \quad (3)$$

¹⁵³ Equation 3 can be seen as a coordinates translation to the new origin (\bar{X}, \bar{Y}) . If we rotate the new coordinate system counterclockwise about O by
¹⁵⁴ angle θ ($0 < \theta \leq 2\pi$) and get the new coordinate system X_o - Y_o , the standard
¹⁵⁵ deviation along X_o axis σ_x and Y_o axis σ_y is calculated as given in Equation
¹⁵⁶ 4 and 5.

$$\sigma_x = \sqrt{\frac{\sum_{i=1}^n (\tilde{y}_i \sin \theta + \tilde{x}_i \cos \theta)^2}{n}} \quad (4)$$

$$\sigma_y = \sqrt{\frac{\sum_{i=1}^n (\tilde{y}_i \cos \theta - \tilde{x}_i \sin \theta)^2}{n}} \quad (5)$$

¹⁵⁸ The long/short axis of SDE is along the direction who has the maxi-
¹⁵⁹ mum/minimum standard deviation. Let σ_{max} and σ_{min} be the length the of
¹⁶⁰ semi-long axis and semi-short axis of SDE. The angle of rotation θ_m of the
¹⁶¹ long/short axis is given by Equation 6 (Yuill, 1971).

$$\tan \theta_m = -\frac{A \pm B}{C} \quad (6)$$

$$A = \sum_{i=1}^n \tilde{x}_i^2 - \sum_{i=1}^n \tilde{y}_i^2 \quad (7)$$

$$C = 2 \sum_{i=1}^n \tilde{x}_i \tilde{y}_i \quad (8)$$

$$B = \sqrt{A^2 + C^2} \quad (9)$$

162 The \pm indicates two rotation angles $\theta_{max}, \theta_{min}$ corresponding to long and
163 short axis.

164 *3.2. Anisotropic Density-Based Clusters*

165 In order to introduce an anisotropic perspective to density-based clus-
166 tering algorithms such as DBSCAN, we have to revise the definition of an
167 *Eps*-neighborhood of a point. First, the original *Eps*-neighborhood of a point
168 in a dataset D is defined by DBSCAN as given by Definition 1.

Definition 1. (*Eps*-neighborhood of a point) *The Eps*-neighborhood $N_{Eps}(p_i)$ of Point p_i is defined as all the points within the scan circle centered at p_i with a radius *Eps*, which can be expressed as:

$$N_{Eps}(p_i) = \{p_j(x_j, y_j) \in D \mid dist(p_i, p_j) \leq Eps\}$$

169 Such scan circle results in an isotropic perspective on clustering. However,
170 as we discuss above, an anisotropic assumption will be more appropriate for
171 some geographic phenomena. Intuitively, in order to introduce anisotropy to
172 DBSCAN, one can employ a scan ellipse instead of a circle to define the
173 *Eps*-neighborhood of each point. Before we give a definition of the *Eps*-
174 ellipse-neighborhood of a point, it is necessary to define a set of points around
175 a point (Search-neighborhood of a point) which is used to derive the scan
176 ellipse; See Definition 2.

177 **Definition 2.** (*Search*-neighborhood of a point) A set of points $S(p_i)$ around
178 Point p_i is called search-neighborhood of Point p_i and can be defined in two
179 ways:

- 180 1. *The Eps*-neighborhood $N_{Eps}(p_i)$ of Point p_i .
- 181 2. *The k-th nearest neighbor KNN*(p_i) of Point p_i . Here $k = MinPts$
182 and $KNN(p_i)$ does not include p_i itself.

183 After determining the search-neighborhood of a point, it is possible to de-
184 fine the *Eps*-ellipse-neighborhood region (See Definition 3) and *Eps*-ellipse-
185 neighborhood (See Definition 4) of each point.

186 **Definition 3.** (*Eps*-ellipse-neighborhood region of a point) An ellipse ER_i
187 is called *Eps*-ellipse-neighborhood region of a point p_i iff:

- 188 1. *Ellipse* ER_i is centered at Point p_i .

- 189 2. Ellipse ER_i is scaled from the standard deviation ellipse SDE_i com-
 190 puted from the Search-neighborhood $S(p_i)$ of Point p_i .
 191 3. $\frac{\sigma_{max}'}{\sigma_{min}'} = \frac{\sigma_{max}}{\sigma_{min}}$;
 192 where $\sigma_{max}, \sigma_{min}'$ and $\sigma_{max}, \sigma_{min}$ are the length of semi-long and semi-
 193 short axis of Ellipse ER_i and Ellipse SDE_i .
 194 4. $Area(ER_i) = \pi ab = \pi Eps^2$

195 According to Definition 3, the Eps -ellipse-neighborhood region of a point
 196 is computed based on the search-neighborhood of a point. Since there are
 197 two definitions of the search-neighborhood of a point (See Definition 2), each
 198 point should have a unique Eps -ellipse-neighborhood region given Eps (using
 199 the first definition in Definition 2) or $MinPts$ (using the second definition in
 200 Definition 2) as long as the search-neighborhood of the current point has at
 201 least two points for the computation of the standard deviation ellipse.

202 **Definition 4.** (*Eps*-ellipse-neighborhood of a point) An *Eps*-ellipse-neighborhood
 203 $EN_{Eps}(p_i)$ of point p_i is defined as all the point inside the eillpse ER_i , which
 204 can be expressed as $EN_{Eps}(p_i) = \{p_j(x_j, y_j) \in D \mid \frac{((y_j - y_i) \sin \theta_{max} + (x_j - x_i) \cos \theta_{max})^2}{a^2} +$
 205 $\frac{((y_j - y_i) \cos \theta_{max} - (x_j - x_i) \sin \theta_{max})^2}{b^2} \leqslant 1\}$.

206 There are two kinds of points in a cluster obtained from DBSCAN: *core*
 207 *point* and *border point*. Core points have at least $MinPts$ points in their
 208 Eps -neighborhood, while border points have less than $MinPts$ points in
 209 their Eps -neighborhood but are *density reachable* from at least one core
 210 point. Our anisotropic clustering algorithm has a similar definition of core
 211 point and border point. The notions of directly anisotropic-density-reachable
 212 and core point are illustrated bellow; see Definition 5.

213 **Definition 5.** (*Directly anisotropic-density-reachable*) A point p_j is directly
 214 anisotropic density reachable from point p_i wrt. Eps and $MinPts$ iff:

- 215 1. $p_j \in EN_{Eps}(p_i)$.
 216 2. $|EN_{Eps}(p_i)| \geq MinPts$. (Core point condition)

217 If point p is directly anisotropic reachable from point q , then point q must
 218 be a core point which has no less than $MinPts$ points in its Eps -ellipse-
 219 neighborhood. Similar to the notion of density-reachable in DBSCAN, the
 220 notion of anisotropic-density-reachable is given in Definition 6.

221 **Definition 6.** (*Anisotropic-density-reachable*) A point p is anisotropic den-
 222 sity reachable from point q wrt. Eps and $MinPts$ if there exists a chain of
 223 points p_1, p_2, \dots, p_n , ($p_1 = q$, and $p_n = p$) such that point p_{i+1} is directly
 224 anisotropic density reachable from p_i .

225 Although anisotropic density reachability is not a symmetric relation, if
 226 such a directly anisotropic density reachable chain exists, then except for point
 227 p_n , the other $n - 1$ points are all core points. If Point p_n is also a core point,
 228 then symmetrically point p_1 is also density reachable from p_n . That means
 229 that if two points p, q are anisotropic density reachable from each other, then
 230 both of them are core points and belong to the same cluster.

231 Equipped with the above definitions, we are able to define our anisotropic
 232 density-based notion of clustering. DBSCAN includes both core points and
 233 border points into its clusters. In our clustering algorithm, only core points
 234 will be treated as cluster points. Border points will be excluded from clusters
 235 and treated as noise points, because otherwise many noise points will be
 236 included into clusters according to experimental results. In short, a cluster
 237 (See definition 7) is defined as a subset of points from the whole points dataset
 238 in which each two points are anisotropic density reachable from another.
 239 Noise points (See Definition 8) are defined as the subset of points from the
 240 entire points dataset for which each point has less than $MinPts$ points in its
 241 Eps -ellipse-neighborhood.

242 **Definition 7.** (*Cluster*) Let D be a points dataset. A cluster C is a no-
 243 empty subset of D wrt. Eps and $MinPts$, iff:

- 244 1. $\forall p \in C, EN_{Eps}(p) \geq MinPts$.
 245 2. $\forall p, q \in C, p, q$ are anisotropic density reachable from each other wrt.
 246 Eps and $MinPts$.

247 A cluster C has two attribute:

248 $\forall p \in C$ and $\forall q \in D$, if p is anisotropic density reachable from q wrt. Eps
 249 and $MinPts$, then

- 250 1. $q \in C$.
 251 2. There must be a directly anisotropic density reachable points chain
 252 $C(q, p)$: p_1, p_2, \dots, p_n , ($p_1 = q$, and $p_n = p$), such that p_{i+1} is directly
 253 anisotropic density reachable from p_i . Then $\forall p_i \in C(q, p), p_i \in C$.

254 **Definition 8.** (*Noise*) Let D be a points dataset. A point p is a noise point
 255 wrt. Eps and $MinPts$, if $p \in D$ and $EN_{Eps}(p) < MinPts$.

256 Let C_1, C_2, \dots, C_k be the clusters of the points dataset D wrt. Eps
 257 and $MinPts$. From Definition 8, if $p \in D$, and $EN_{Eps}(p) < MinPts$, then
 258 $\forall C_i \in \{C_1, C_2, \dots, C_k\}, p \notin C_i$.

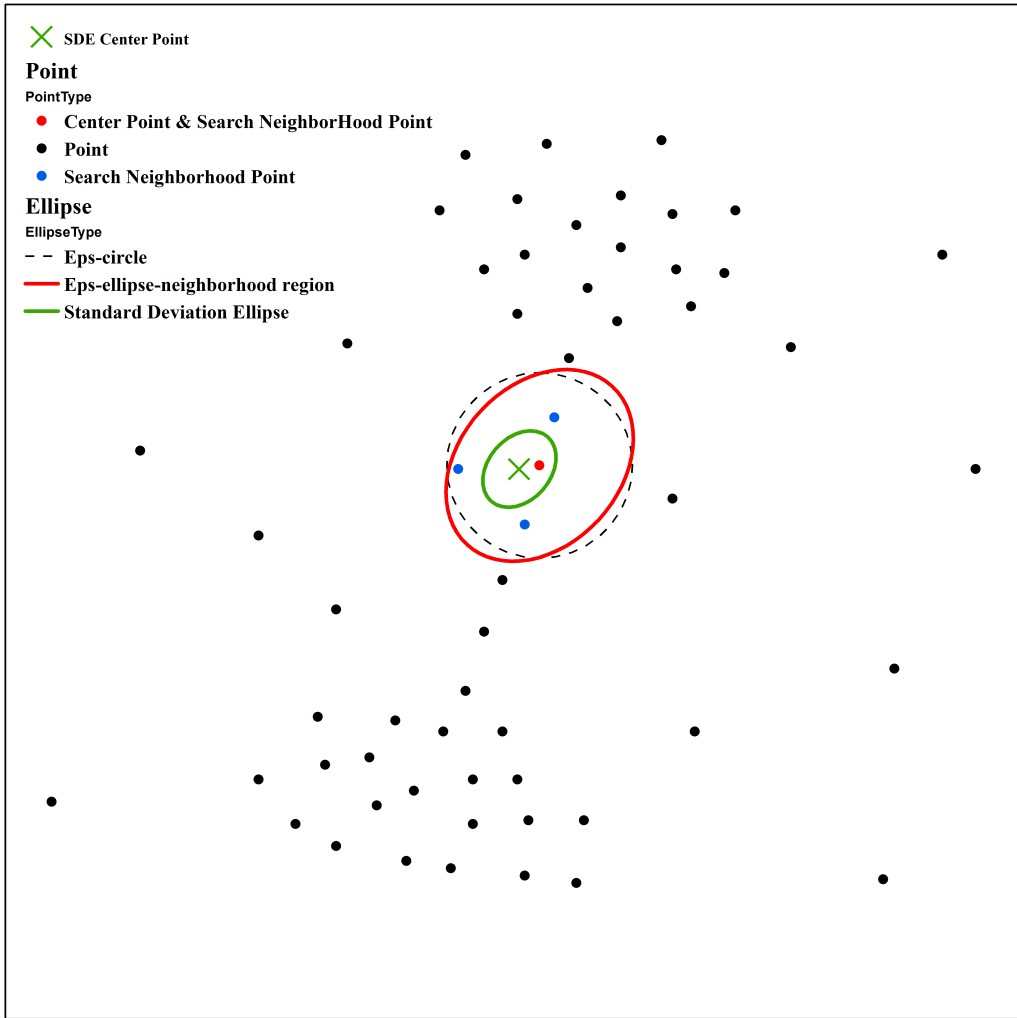


Figure 2: Illustration for ADCN-Eps

259 According to Definition 2, and in contrast to a simple scan circle, there
 260 are at least two ways to define a search neighborhood of the center point

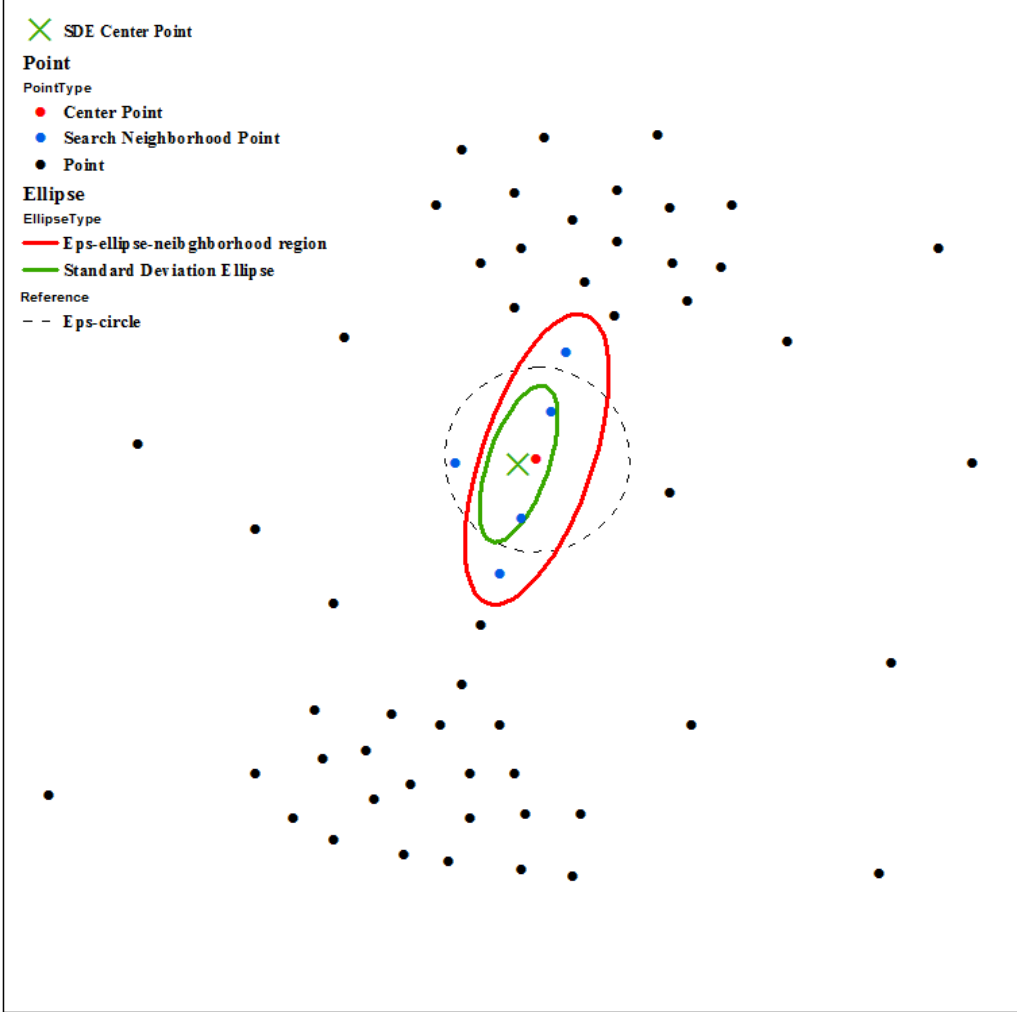


Figure 3: Illustration for ADCN-KNN

261 p_i . Thus, ADCN can be divided into a ADCN-Eps variant that uses Eps -
 262 neighborhood $N_{Eps}(p_i)$ as the search neighborhood and ADCN-KNN that
 263 uses k -th nearest neighbors $KNN(p_i)$ as the search neighborhood. Figures 2
 264 and 3 illustrates the related definitions for ADCN-Eps and ADCN-KNN. The
 265 red points in both figures represent current center points. The blue points
 266 indicate the two different search neighborhoods of the corresponding center
 267 points according to Definition 2. Note that for ADCN-Eps, the center point
 268 is also part of its search neighborhood which is not true for ADCN-KNN.

269 The green ellipses and green crosses stand for the standard deviation ellipses
270 constructed from the corresponding search neighborhood and their center
271 points. The red ellipses are Eps -ellipse-neighborhood regions while the dash
272 line circles indicate a DBSCAN-like scan circle. As can be seen, ADCN-KNN
273 will exclude the point to the left of the linear *bridge*-pattern while DBSCAN
274 would include it.

275 *3.3. ADCN Algorithms*

276 From the definitions provided above it follows that our *anisotropic density-*
277 *based clustering with noise* algorithm takes the same parameters ($MinPts$
278 and Eps) as DBSCAN and that they have to be decided before clustering.
279 This is for good reasons, as the proper selection of DBSCAN parameters
280 has been well studied and ADCN can easily replace DBSCAN without any
281 changes to established workflows.

282 As shown in Algorithm 1, ADCN starts with an arbitrary point p_i in
283 a points dataset D and discovers all the *core* points which are anisotropic
284 density reachable from point p_i . According to Definition 2, there are two
285 ways to get the search neighborhood of point p_i which will result in differ-
286 ent Eps -ellipse-neighborhood $EN_{Eps}(p_j)$ based on the derived Eps -ellipse-
287 neighborhood-region in Algorithm 2. Hence, ADCN can be implemented by
288 two algorithms (ADCN-Eps, ADCN-KNN). Algorithm 2 needs to take care
289 of situations when all points of the Search-neighborhood $S(p_i)$ of Point p_i
290 are *strictly* on the same line. In this case, the short axis of Eps -ellipse-
291 neighborhood region ER_i becomes *zero* and its long axis become *Infinity*.
292 This means $EN_{Eps}(p_i)$ is diminished to a straight line. The process of con-
293 structing Eps -ellipse-neighborhood $EN_{Eps}(p_i)$ of Point p_i becomes a point-
294 on-line query.

295 According to Algorithm 3, ADCN-Eps uses the Eps -neighborhood $N_{Eps}(p_i)$
296 of point p_i as the search neighborhood which will be used later to construct
297 the standard deviation ellipse. In contrast, ADCN-KNN (Algorithm 4) uses
298 a k-th nearest neighborhood of point p_i as the search neighborhood. Here
299 point p_i will not be included in its k-th nearest neighborhood. As can be
300 seen, the run times of ADCN-Eps and ADCN-KNN are heavily dominated
301 by the search-neighborhood query which is executed on each point. Hence,
302 the time complexities of ADCN, DBSCAN, and OPTICS are $O(n^2)$ without
303 a spatial index and $O(n \log n)$ otherwise.

Algorithm 1: ADCN(D , $MinPts$, Eps)

Input : A set of n points $D(X, Y)$; $MinPts$; Eps ;
Output: Clusters with different labels $C_i[]$; A set of noise points $Noi[]$

```
1 foreach point  $p_i(x_i, y_i)$  in the set of points  $D(X, Y)$  do
2     | Mark  $p_i$  as Visited;
3     | //Get  $Eps$ -ellipse-neighborhood  $EN_{Eps}(p_i)$  of  $p_i$ 
4     | ellipseRegionQuery( $p_i$ ,  $D$ ,  $MinPts$ ,  $Eps$ );
5     | if  $|EN_{Eps}(p_i)| < MinPts$  then
6         |   | Add  $p_i$  to the noise set  $Noi[]$ ;
7     | else
8         |   | Create a new Cluster  $C_i[]$ ;
9         |   | Add  $p_i$  to  $C_i[]$ ;
10        |   | foreach point  $p_j(x_j, y_j)$  in  $EN_{Eps}(p_i)$  do
11            |       | if  $p_j$  is not visited then
12                |           |   | Mark  $p_j$  as visited;
13                |           |   | //Get  $Eps$ -ellipse-neighborhood  $EN_{Eps}(p_j)$  of Point  $p_j$ 
14                |           |   | ellipseRegionQuery( $p_j$ ,  $D$ ,  $MinPts$ ,  $Eps$ );
15                |           |   | if  $|EN_{Eps}(p_j)| \geq MinPts$  then
16                    |               |   | Let  $EN_{Eps}(p_i)$  as the merged set of  $EN_{Eps}(p_i)$  and
17                    |               |   |  $EN_{Eps}(p_j)$ ;
18                    |               |   | Add  $p_j$  to current cluster  $C_i[]$ ;
19                |           |   | else
20                    |               |   |   | Add  $p_j$  to the noise set  $Noi[]$ ;
21                |           |   | end
22            |       | end
23        |   | end
24    | end
```

304 **4. Experiments and Performance Evaluation**

305 In this section, we will evaluate the performance of ADCN from two per-
306 spectives: clustering quality and clustering efficiency. In contrast to the scan
307 circle of DBSCAN, there are at least two ways to determine an anisotropic
308 neighborhood. This leads to two realizations of ADCN, namely ADCN-KNN
309 and ADCN-Eps. We will evaluate their performance using DBSCAN and

Algorithm 2: ellipseRegionQuery($p_i, D, MinPts, Eps$)

Input : $p_i, D, MinPts, Eps$
Output: Eps -ellipse-neighborhood $EN_{Eps}(p_i)$ of Point p_i

1 //Get the Search-neighborhood $S(p_i)$ of Point p_i . ADCN-Eps and
ADCN-KNN use different functions.
2 ADCN-Eps: searchNeighborhoodEps(p_i, D, Eps); ADCN-KNN:
searchNeighborhoodKNN($p_i, D, MinPts$);
3 Compute the standard deviation ellipse SDE_i base on the
Search-neighborhood $S(p_i)$ of Point p_i ;
4 Scale Ellipse SDE_i to get the Eps -ellipse-neighborhood region ER_i of
Point p_i to make sure $Area(ER_i) = \pi \times Eps^2$;
5 **if** *The length of short axis of $ER_i == 0$* **then**
6 // the Eps -ellipse-neighborhood region ER_i of Point p_i is
 diminished to a straight line. Get Eps -ellipse-neighborhood
 $EN_{Eps}(p_i)$ of Point p_i by finding all points on this straight line
 ER_i ;
7 **else**
8 // the Eps -ellipse-neighborhood region ER_i of Point p_i is an
 ellipse. Get Eps -ellipse-neighborhood $EN_{Eps}(p_i)$ of Point p_i by
 finding all the points inside Ellipse ER_i ;
9 **end**
10 return $EN_{Eps}(p_i)$;

310 OPTICS as baselines. We selected OPTICS as an additional baseline as it
311 is commonly used to address some of DBSCAN's shortcomings with respect
312 to varying densities.

313 According to the research contributions outlined in Section 1, we intend
314 to establish **(1)** that at least one of the ADCN variants performs as good
315 as DBSCAN (and OPTICS) for cases that do not explicitly benefit from an
316 anisotropic perspective; **(2)** that the aforementioned variant performs better
317 than the baselines for cases that *do* benefit from an anisotropic perspective;
318 and finally **(3)** that the test cases include point patterns typically used to test
319 density-based clustering algorithms as well as *real-world* cases that highlight
320 the need for developing ADCN in the first place. In addition, we will show
321 runtime results for all four algorithms.

Algorithm 3: searchNeighborhoodEps(p_i, D, Eps)

Input : p_i, D, Eps
Output: the Search-neighborhood $S(p_i)$ of Point p_i

```
1 // This function is used in ADCN-Eps // Get all the points whose
   distance from Point  $p_i$  is less than  $Eps$ 
2 foreach point  $p_j(x_j, y_j)$  in the set of points  $D(X, Y)$  do
3   | if  $\sqrt{(x_i - x_j)^2 + (y_i - y_j)^2} \leq Eps$  then
4     |   Add Point  $p_j$  to  $S(p_i)$ ;
5 end
6 return  $S(p_i)$ ;
```

322 *4.1. Experiment Designs*323 We have designed several spatial point patterns as test cases for our ex-
324 periments. More specifically, we generated 20 test cases with 3 different noise
325 settings for each of them. These consist of 12 synthetic and 8 real-world use
326 cases which results in a total of **60** case studies. Note that our test cases
327 do not only contain linear features such as road networks but also cases that
328 are typically used to evaluate algorithms such as DBSCAN, e.g., clusters of
329 ellipsoid and rectangular shapes.330 In order to simulate a “ground truth” for the synthetic cases, we created
331 polygons to indicate different clusters and randomly generated points within
332 these polygons and outside of them. We took a similar approach for the
333 eight real-world cases. The only difference is that the polygons for real world
334 cases have been generated from buffer zones with a 3-meter radius of the
335 real-world features, e.g., existing road networks. This allows us to simulate
336 patterns that typically occur in geo-tagged social media data.337 Although we use this approach to simulate the corresponding spatial point
338 process, the distinction between clustered points and noise points in the
339 resulting spatial point patterns may not be so obvious even from a human’s
340 perspective. To avoid cases in which it is unreasonable to expect algorithms
341 and humans to differentiate between noise and pattern, we introduced a
342 clipping buffer of 0m, 5m, and 10m. For comparison, the typical position
343 accuracy of GPS sensors on smartphones and GPS collars for wildlife tracking
344 is about 3-15 meters (Wing et al., 2005)(and can decline rapidly in urban
345 canyons).

346 The generated spatial point patterns of 12 synthetic and 8 real-world use

Algorithm 4: searchNeighborhoodKNN($p_i, D, MinPts$)

Input : $p_i; D; MinPts$

Output: the Search-neighborhood $S(p_i)$ of Point p_i

1 // This function is used in ADCN-KNN // Get the Kth nearest neighbor of Point p_i excluding p_i itself

2 KNNArray = new Array($MinPts$);

3 distanceArray = new Array($|D|$);

4 KNNLabelArray = new Array($|D|$);

5 **foreach** point $p_j(x_j, y_j)$ in the set of points $D(X, Y)$ **do**

6 | KNNLabelArray[j] = 0;

7 | distanceArray[j] = $\sqrt{(x_i - x_j)^2 + (y_i - y_j)^2}$;

8 | **if** $j == i$ **then**

9 | | KNNLabelArray[j] = 1;

10 **end**

11 **foreach** k in $0:(MinPts - 1)$ **do**

12 | minDist = Infinity;

13 | minDistID = 0;

14 | **foreach** j in $0:|D|$ **do**

15 | | **if** $KNNLabelArray[j] != 1$ **then**

16 | | | **if** $minDist > distanceArray[j]$ **then**

17 | | | | minDist = distanceArray[j];

18 | | | minDistID = j;

19 | | **end**

20 | | KNNLabelArray[minDistID] = 1;

21 | | KNNArray[k] = minDistID;

22 | | Add the point with minDistID as ID to $S(p_i)$;

23 **end**

24 **return** $S(p_i)$;

347 cases with 0m buffer distance are shown in the first column of Figure 5 and
348 Figure 6. Note that in all test cases, points generated from different polygons
349 are pre-labeled with different cluster IDs which are indicated by different
350 colors in the first column of Figure 5 and Figure 6. Points generated outside
351 polygons are pre-labeled as *noise* which are shown in *black*. These generated
352 spatial point patterns serve as *ground truth* which are used in our clustering
353 quality evaluation experiments.

354 In order to demonstrate the strengthen of ADCN, we need to compare
355 the performance of ADCN with that of DBSCAN and OPTICS from two
356 perspectives: clustering quality and clustering efficiency. The experiment
357 designs are as follow:

- 358 • As for clustering quality evaluation, we use several clustering quality
359 indices to quantify how good the clustering results are. In this work,
360 we use Normalized Mutual Information (NMI) and the Rand Index.
361 We will explain these two indices in detail in Section 4.3. We stepwise
362 tested every possible parameter combinations of Eps , $MinPts$ computa-
363 tionally on each test case. For each clustering algorithm, we select the
364 parameter combination which has the highest NMI or Rand index. By
365 comparing the maximum of NMI and Rand index across different clus-
366 tering algorithms in each test case, we can find out the best clustering
367 technique.
- 368 • As for clustering efficiency evaluation, we generate spatial point pat-
369 terns with different numbers of points by using the polygons of each
370 test case mentioned earlier. For each clustering algorithm and each
371 number of points setting, we computed the average runtime. By con-
372 structing a runtime curve of each clustering algorithm, we are able to
373 compare their runtime efficiency.

374 *4.2. Test Environment*

375 In order to compare the performance of ADCN with that of DBSCAN and
376 OPTICS, we developed a JavaScript test environment to generate patterns
377 and compare the results. It allows us to generate use cases in a Web browser,
378 such as Firefox or Chrome, or load them from a GIS, change noise settings,
379 determine DBSCAN’s Eps via a KNN distance plot, perform different eval-
380 uations, compute runtimes, index the data via an R-tree, and save and load
381 the data. Consequently, what matters is the *runtime behavior*, not the ex-
382 act performance (for which JavaScript would not be a suitable choice). All
383 cases have been performed on a *cold* setting, i.e., without any caching using
384 an Intel i5-5300U CPU with 8 GB RAM on an Ubuntu 16.04 system. This
385 Javascript test environment as well as all the test cases can be downloaded
386 from here².

²<http://stko.geog.ucsb.edu/adcn/>

387 Figure 4 shows a snapshot of this test environment. The system has two
 388 main panels. The map panel on the left side is an interactive canvas in which
 389 the user can click and create data points. The tool bar on the right side is
 390 composed of input boxes, selection boxes, and buttons which are divided
 391 into different groups. Each group is used for a specific purpose, which will
 392 be discussed as below.

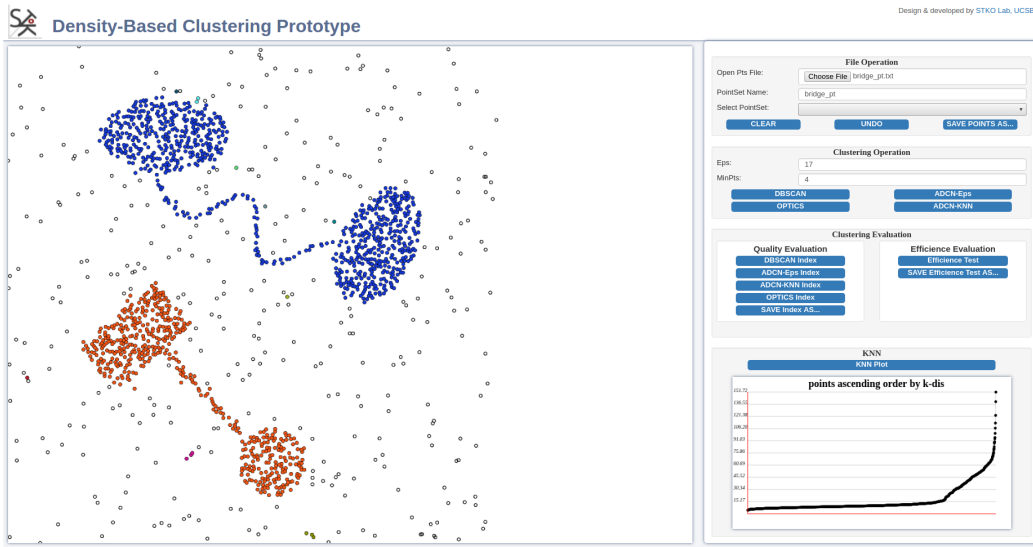


Figure 4: The Density-Based Clustering Test Environment

393 The “File Operation” tool group is used for point dataset manipulation.
 394 For simplicity, our environment defines a simple format for point datasets.
 395 Conceptually, a point dataset is a table containing the coordinates of points,
 396 their ground truth memberships, and the memberships produced during the
 397 experiments. The ground truth and experimental memberships are then
 398 compared to evaluate the cluster algorithms. The “Open Pts File” box is
 399 used for loading point datasets produced by other GIS. The data points can
 400 also be abstract points which represent objects, such as documents (Fabrikant
 401 and Montello, 2008), in a feature space. The prototype takes the coordinates
 402 of points and maps out these points after rescaling their coordinates based
 403 on the size of the map panel. During the clustering process it uses Euclidean
 404 distance as the distance measure.

405 The “Clustering Operation” tool group is used to operate clustering tasks.
 406 The “Eps” and “MinPts” input boxes let users enter the clustering param-

407 eters for all clustering algorithms. The “DBSCAN”, “OPTICS”, “ADCN-
408 Eps”, “ADCN-KNN” buttons are for running the algorithms. As for the
409 implementation of DBSCAN and OPTICS, we used a JavaScript clustering
410 library from GitHub ³. This library has basic implementations of DBSCAN,
411 OPTICS, K-MEANS, and some other clustering algorithms without any spa-
412 tial indexes. Our ADCN-KNN and ADCN-Eps algorithms were implemented
413 using the same data structures as used in the library. Such an implemen-
414 tation ensures that the evaluation result will reflect the differences of the
415 algorithms rather than be affected by the specific data structures used in the
416 implementations. Finally, we implemented an R-tree spatial index to accel-
417 erate the neighborhood search. We have used the R-tree JavaScript library
418 from GitHub ⁴.

419 The “Clustering Evaluation” tool group is composed of “Quality Evalu-
420 ation” and “Efficiency Evaluation” subgroups. As for the clustering quality
421 evaluation, we implemented two metrics, Normalized mutual Information
422 (NMI) and Rand Index, to quantify the goodness of the clustering results.
423 The first four buttons in this subgroup will run the corresponding clustering
424 algorithm on the current dataset based on all possible parameter combina-
425 tions. They will compute two clustering evaluation indexes for each clustering
426 result. The “SAVE Index As...” button will save these results to a text file.

427 Efficiency evaluation is another important part for comparing clustering
428 algorithms. The “Efficiency Evaluation” button will run these four clustering
429 algorithms on datasets with different sizes. The “SAVE Efficiency Test As...”
430 button can be further used to save the result into a text file.

431 Finally, the “KNN” tool group is used to draw the k_{th} nearest neighbor
432 plot (KNN plot) of the current dataset based on the $MinPts$ parameter spec-
433 ified by the user. For each point, the KNN plot obtains the distance between
434 the current point and its k_{th} nearest point (here K is $MinPts$). Then it
435 ranks these k_{th} nearest distance of each point in an ascending order. The
436 KNN plot can be used for estimating the appropriate Eps for the current
437 point dataset given $MinPts$. More details this estimation can be found in the
438 original DBSCAN paper (Ester et al., 1996).

439 Note that we provide the test environment to make our results repro-
440 ducible and to offer a reusable implementation of ADCN, without implying

³<https://github.com/uhho/density-clustering>

⁴<https://github.com/imbcmndth/RTree>

441 that JavaScript would be the language of choice for future, large-scale appli-
 442 cations of ADCN.

443 *4.3. Evaluation of Clustering Quality*

444 We use two clustering quality indices - the normalized mutual information
 445 (NMI) and the Rand Index - to measure the quality of clustering results of
 446 all algorithms. NMI originates from information theory and has been revised
 447 as an objective function for clustering ensembles (Strehl and Ghosh, 2002).
 448 NMI evaluates the accumulated mutual information shared by the clusters
 449 from different clustering algorithms. Let n be the number of points in a point
 450 datasets D . $X = (X_1, X_2, \dots, X_r)$ and $Y = (Y_1, Y_2, \dots, Y_s)$ are two clustering
 451 results from the same or different clustering algorithms. Note that noise
 452 points will be treated as their own cluster. Let $n_h^{(x)}$ be the number of points
 453 in cluster X_h and $n_l^{(y)}$ the number of points in cluster Y_l . Let $n_{h,l}^{(x,y)}$ be the
 454 number of points in the intersect of cluster X_h and Y_l . Then the normalized
 455 mutual information $\Phi^{(NMI)}(X, Y)$ is defined in Equation 10 as the similarity
 456 between two clustering results X and Y :

$$\Phi^{(NMI)}(X, Y) = \frac{\sum_{h=1}^r \sum_{l=1}^s n_{h,l}^{(x,y)} \log \frac{n \cdot n_{h,l}^{(x,y)}}{n_h^{(x)} \cdot n_l^{(y)}}}{\sqrt{(\sum_{h=1}^r n_h^{(x)} \log \frac{n_h^{(x)}}{n})(\sum_{l=1}^s n_l^{(y)} \log \frac{n_l^{(y)}}{n})}} \quad (10)$$

457 Rand Index (Rand, 1971) is another objective function for clustering en-
 458 sembles from a different perspective. It evaluates to which degree two clus-
 459 tering algorithms share the same relationships between points. Let a be the
 460 number of pairs of points in D that are in the same clusters in X and in
 461 the same cluster in Y . b is the number of pairs of points in D that are in
 462 different clusters in X and Y . c is the number of pairs of points in D that
 463 are in the same clusters in X and in different cluster in Y . Finally, d is the
 464 number of pairs of points in D that are in different clusters in X and in the
 465 same cluster in Y . The Rand Index $\Phi^{(Rand)}(X, Y)$ is then defined as given
 466 by Equation 11:

$$\Phi^{(Rand)}(X, Y) = \frac{a + b}{a + b + c + d} \quad (11)$$

467 For both NMI and Rand index, larger values indicate higher similarity
 468 between two clustering results. If a ground truth is available, both NMI

469 and Rand can be used to compute the similarity between the result of an
470 algorithms and the corresponding ground truth. This is called the *extrinsic*
471 *method* (Han et al., 2011).

472 We use the aforementioned 20 test cases to evaluate the clustering qual-
473 ity of DBSCAN, ADCN-Eps, ADCN-KNN, and OPTICS. All of these four
474 algorithms take the same parameters (*Eps*, *MinPts*). As there are no estab-
475 lished methods to determine the best overall parameter combination (we use
476 KNN distance plots to estimate Eps) with respect to NMI and Rand Index,
477 we stepwise tested every possible parameter combinations of *Eps*, *MinPts*
478 computationally. An interactive 3D visualization of the NMI and Rand index
479 results with changing *Eps* and *MinPts* for the *spiral* case with 0m buffer
480 distance can be accessed online ⁵. Table 1 shows the maximum NMI and
481 Rand Index results for the four algorithms over all test cases. Note that for
482 each case, the best parameter combination with the maximum NMI does not
483 necessarily yields the maximum Rand Index. However, among all of these 60
484 cases, there are 39, 35, 27, 39 cases for DBSCAN, ADCN-Eps, ADCN-KNN,
485 OPTICS in which the best parameter combination for the maximum NMI is
486 also the maximum Rand Index. For those cases where parameter combina-
487 tions of maximum NMI and maximum Rand do not match, their parameters
488 tend to be close to each other because NMI and Rand values are changing
489 continuously while *Eps* and *MinPts* increase. This indicates that NMI and
490 Rand Index have a medium to high similarity in terms of measuring the
491 clustering quality.

492 As for the 60 test cases, ADCN-KNN has a higher maximum NMI/Rand
493 Index than DBSCAN in **55** cases and has a higher maximum NMI/Rand
494 Index than OPTICS in **55** cases; see also Figures 7 and 8. Even more,
495 ADCN-KNN has a higher maximum NMI/Rand Index than ADCN-Eps in **31**
496 cases; see Table 2. This indicates that ADCN-KNN gives the best clustering
497 results among the tested algorithms. Our test cases do not only contain linear
498 features but also cases that are typically used to evaluate algorithms such as
499 DBSCAN, e.g., clusters of ellipsoid and rectangular shapes. In fact, these are
500 the only cases were DBSCAN slightly out-competes ADCN-KNN, i.e., the
501 maximum NMI/Rand Index of ADCN-KNN and DBSCAN are comparable.
502 Summing up, ADCN-KNN performs better than all other algorithms when
503 dealing with anisotropic cases and equally well as DBSCAN for isotropic

⁵<http://stko.geog.ucsb.edu/adcn/>

504 cases. In the following paragraphs, we will use ADCN-KNN and ADCN
505 interchangeably.

506 Figure 5 and 6 show the point patterns as well as the best clustering
507 results of all algorithms for the twelve synthesis cases and eight real-world
508 cases without buffering, i.e., with the 0m buffer distance. By comparing
509 best clustering results of these four algorithms, we can find some interesting
510 patterns: 1) *Connecting clusters along local directions*: ADCN has a better
511 ability to detect the local direction of spatial point patterns and connect the
512 clusters along this direction; 2) *Noise filtering*: ADCN does better in filtering
513 out noise points. A good example of *connecting clusters along local directions*
514 is the *ellipseWidth* case in Figure 5. As for the thinnest cluster in the bottom,
515 the other 3 algorithms except ADCN-KNN extract multiple clusters from
516 these points while ADCN-KNN is able to “connect” these clusters to a single
517 one. Many cases show the *noise filtering* advantage of ADCN. For example,
518 the *bridge* case, the *multiBridge* case in Figure 5, and the *Brooklyn Bridge*
519 case in Figure 6, reveal that ADCN is better at detecting and filtering out
520 noise points along bridge-like features.

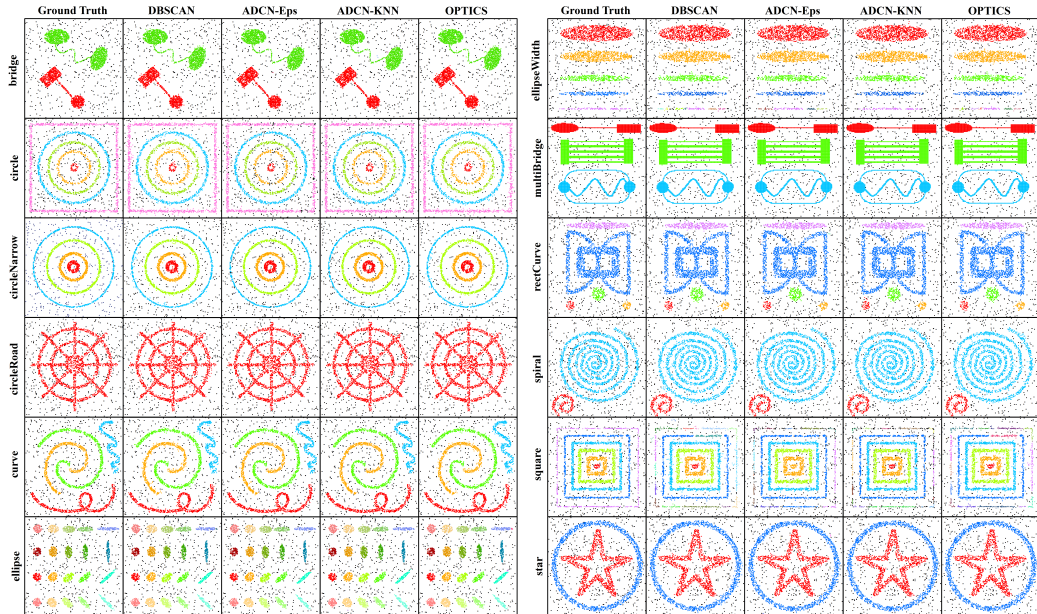


Figure 5: Ground truth and best clustering result comparison for 12 synthesis cases.

521 4.4. Evaluation of Clustering Efficiency

522 Finally, this subsection discusses runtime differences of the four tested
523 algorithms. Without a spatial index, the time complexity of all algorithms
524 is $O(n^2)$. Eps -neighborhood queries consume the major part of the run time
525 of density-based clustering algorithms (Ankerst et al., 1999), and, therefore,
526 also of ADCN-KNN and ADCN-Eps in terms of Eps -ellipse-neighborhood
527 queries. Hence, we implemented an R-tree to accelerate the neighborhood
528 queries for all algorithms. This changes their time complexity to $O(n \log n)$.

529 In order to enable a comprehensible comparison of the run times of all
530 algorithms on different sizes of point datasets, we performed a batch of per-
531 formance tests. The polygons from the 20 cases shown above have been used
532 to generated point datasets of different sizes ranging from 500 to 10000 in
533 500 step intervals. The ratio of noise points to cluster points is set to 0.25.
534 Eps , $MinPts$ are set to 15, 5 for all of these experiments. The average run
535 times for the same size of point datasets is depicted in Figure 9.

536 Unsurprisingly, the runtime of all algorithms increases as the number of
537 points increases. The runtime of ADCN-KNN is larger than that of DBSCAN
538 and similar that of OPTICS. As the size of the point dataset increases, the
539 ratio of the runtimes of ADCN-KNN to DBSCAN decrease from 2.80 to
540 1.29. The original OPTICS paper states a 1.6 runtime factor compared
541 to DBSCAN. The used OPTICS library failed on datasets exceeding 5500
542 points. We also fit the runtime data to the $xlog(x)$ function. Figure 9 shows
543 the fitted curves and functions of each clustering algorithm. We can see that
544 all R^2 of these functions are larger than 0.95 which means that the $xlog(x)$
545 function well captures the trends of the real runtime data of these clustering
546 algorithms. For ADCN, our implementation tests for point-in-circle for the
547 radius of the major axis before computing point-in-ellipse to significantly
548 reduce the runtime. Further implementation optimizations are possible but
549 out of scope of this paper.

550 5. Summary and Outlook

551 In this work, we proposed an anisotropic density-based clustering algo-
552 rithm (ADCN). Both synthetic and real-world cases have been used to verify
553 the clustering quality and efficiency of our algorithm compared to DBSCAN
554 and OPTICS. We demonstrate that ADCN-KNN outperforms DBSCAN and
555 OPTICS for the detection of anisotropic spatial point patterns and performs

556 equally well in cases that do not explicitly benefit from an anisotropic per-
557 spective. ADCN has the same time complexity as DBSCAN and OPTICS,
558 namely $O(n \log n)$ when using a spatial index and $O(n^2)$ otherwise. With
559 respect to the average runtime, the performance of ADCN is comparable
560 to OPTICS. Our algorithm is particularly suited for linear features such as
561 typically encountered in urban structures. Application areas include but are
562 not limited to cleaning and clustering geotagged social media data, e.g., from
563 Twitter, Flickr or Strava, analyzing trajectories collected from car sensors,
564 wildlife tracking, and so forth. Future work will focus on improving the im-
565 plementation of ADCN as well as on studying cognitive aspects of clustering
566 and noise detection of linear features.

567 References

- 568 Ankerst, M., Breunig, M. M., Kriegel, H.-P., Sander, J., 1999. OPTICS:
569 ordering points to identify the clustering structure. In: Proceedings of
570 ACM SIGMOD Conference. Vol. 28. ACM, pp. 49–60.
- 571 Barden, L., 1963. Stresses and displacements in a cross-anisotropic soil.
572 Geotechnique 13 (3), 198–210.
- 573 Birant, D., Kut, A., 2007. ST-DBSCAN: An algorithm for clustering spatial–
574 temporal data. Data & Knowledge Engineering 60 (1), 208–221.
- 575 Boisvert, J., Manchuk, J., Deutsch, C., 2009. Kriging in the presence of lo-
576 cally varying anisotropy using non-euclidean distances. Mathematical Geo-
577 sciences 41 (5), 585–601.
- 578 Borah, B., Bhattacharyya, D., 2004. An improved sampling-based DBSCAN
579 for large spatial databases. In: Proceedings of International Conference on
580 Intelligent Sensing and Information. IEEE, pp. 92–96.
- 581 Comaniciu, D., Meer, P., 2002. Mean shift: A robust approach toward fea-
582 ture space analysis. IEEE Transactions on Pattern Analysis and Machine
583 Intelligence 24 (5), 603–619.
- 584 Damiani, M. L., Issa, H., Fotino, G., Heurich, M., Cagnacci, F., 2016. In-
585 troducing presenceand stationarity indexto study partial migration pat-
586 terns: an application of a spatio-temporal clustering technique. Interna-
587 tional Journal of Geographical Information Science 30 (5), 907–928.

- 588 Davies, D. L., Bouldin, D. W., 1979. A cluster separation measure. *IEEE*
589 *Transactions on Pattern Analysis and Machine Intelligence* (2), 224–227.
- 590 Deng, M., Liu, Q., Cheng, T., Shi, Y., 2011. An adaptive spatial clustering
591 algorithm based on delaunay triangulation. *Computers, Environment and*
592 *Urban Systems* 35 (4), 320–332.
- 593 Duckham, M., Kulik, L., Worboys, M., Galton, A., 2008. Efficient generation
594 of simple polygons for characterizing the shape of a set of points in the
595 plane. *Pattern Recognition* 41 (10), 3224–3236.
- 596 DErcole, R., Mateu, J., 2013. On wavelet-based energy densities for spa-
597 tial point processes. *Stochastic environmental research and risk assessment*
598 27 (6), 1507–1523.
- 599 Ester, M., Kriegel, H.-P., Sander, J., Xu, X., 1996. A density-based algorithm
600 for discovering clusters in large spatial databases with noise. In: Proceed-
601 ings of 2nd International Conference on KDD. Vol. 96. pp. 226–231.
- 602 Fabrikant, S. I., Montello, D. R., 2008. The effect of instructions on dis-
603 tance and similarity judgements in information spatializations. *Internation-
604 al Journal of Geographical Information Science* 22 (4), 463–478.
- 605 Fortin, M.-j., Dale, M. R., Ver Hoef, J. M., 2002. Spatial analysis in ecology.
606 *Encyclopedia of environmetrics*.
- 607 Gao, S., Janowicz, K., Montello, D. R., Hu, Y., Yang, J.-A., McKenzie,
608 G., Ju, Y., Gong, L., Adams, B., Yan, B., 2017. A data-synthesis-driven
609 method for detecting and extracting vague cognitive regions. *International
610 Journal of Geographical Information Science* 31 (6), 1245–1271.
- 611 Han, J., Kamber, M., Pei, J., 2011. Data mining: concepts and techniques.
612 Elsevier.
- 613 Hanwell, D., Mirmehdi, M., 2014. QUAC: Quick unsupervised anisotropic
614 clustering. *Pattern Recognition* 47 (1), 427–440.
- 615 Hoek, E., 1964. Fracture of anisotropic rock. *Journal of the South African
616 Institute of Mining and Metallurgy* 64 (10), 501–523.

- 617 Hu, Y., Gao, S., Janowicz, K., Yu, B., Li, W., Prasad, S., 2015. Extracting
618 and understanding urban areas of interest using geotagged photos. Com-
619 puters, Environment and Urban Systems 54, 240–254.
- 620 Huang, Q., 2017. Mining online footprints to predict users next location.
621 International Journal of Geographical Information Science 31 (3), 523–
622 541.
- 623 Huang, Q., Wong, D. W., 2015. Modeling and visualizing regular human
624 mobility patterns with uncertainty: an example using twitter data. Annals
625 of the Association of American Geographers 105 (6), 1179–1197.
- 626 Huang, Q., Wong, D. W., 2016. Activity patterns, socioeconomic status and
627 urban spatial structure: what can social media data tell us? International
628 Journal of Geographical Information Science 30 (9), 1873–1898.
- 629 Isaaks, E. H., Srivastava, R. M., 1989. Applied geostatistics. No. 551.72 I86.
630 Oxford University Press.
- 631 Jurdak, R., Zhao, K., Liu, J., AbouJaoude, M., Cameron, M., Newth,
632 D., 2015. Understanding human mobility from twitter. PloS one 10 (7),
633 e0131469.
- 634 Liu, P., Zhou, D., Wu, N., 2007. VDBSCAN: varied density based spatial
635 clustering of applications with noise. In: 2007 International conference on
636 service systems and service management. IEEE, pp. 1–4.
- 637 Machuca-Mory, D. F., Deutsch, C. V., 2013. Non-stationary geostatistical
638 modeling based on distance weighted statistics and distributions. Mathe-
639 matical Geosciences 45 (1), 31–48.
- 640 MacQueen, J., et al., 1967. Some methods for classification and analysis of
641 multivariate observations. In: Proceedings of the fifth Berkeley symposium
642 on mathematical statistics and probability. Vol. 1. Oakland, CA, USA., pp.
643 281–297.
- 644 Mai, G., Janowicz, K., Hu, Y., Gao, S., 2016. Adcn: an anisotropic density-
645 based clustering algorithm. In: Proceedings of the 24th ACM SIGSPA-
646 TIAL International Conference on Advances in Geographic Information
647 Systems. ACM, p. 58.

- 648 Møller, J., Toftaker, H., 2014. Geometric anisotropic spatial point pattern
649 analysis and cox processes. Scandinavian Journal of Statistics 41 (2), 414–
650 435.
- 651 Moreira, A., Santos, M. Y., 2007. Concave hull: A k-nearest neighbours
652 approach for the computation of the region occupied by a set of points.
653 In: Proceedings of the International Conference on Computer Graphics
654 Theory and Applications. pp. 61–68.
- 655 Rajala, T. A., Särkkä, A., Redenbach, C., Sormani, M., 2016. Estimating
656 geometric anisotropy in spatial point patterns. Spatial Statistics 15, 100–
657 114.
- 658 Rand, W. M., 1971. Objective criteria for the evaluation of clustering meth-
659 ods. Journal of the American Statistical association 66 (336), 846–850.
- 660 Rocha, J. A. M., Times, V. C., Oliveira, G., Alvares, L. O., Bogorny, V., 2010.
661 DB-SMoT: A direction-based spatio-temporal clustering method. In: 2010
662 5th IEEE International Conference Intelligent Systems. IEEE, pp. 114–
663 119.
- 664 Sander, J., Ester, M., Kriegel, H.-P., Xu, X., 1998. Density-based clustering
665 in spatial databases: The algorithm GDBSCAN and its applications. Data
666 mining and knowledge discovery 2 (2), 169–194.
- 667 Stefanakis, E., 2007. NET-DBSCAN: clustering the nodes of a dynamic linear
668 network. International Journal of Geographical Information Science 21 (4),
669 427–442.
- 670 Strehl, A., Ghosh, J., 2002. Cluster ensembles—a knowledge reuse framework
671 for combining multiple partitions. Journal of machine learning research
672 3 (Dec), 583–617.
- 673 Stroet, C. B. t., Snepvangers, J. J., 2005. Mapping curvilinear structures
674 with local anisotropy kriging. Mathematical geology 37 (6), 635–649.
- 675 Tsai, C.-F., Liu, C.-W., 2006. KIDBSCAN: a new efficient data clustering
676 algorithm. In: International Conference on Artificial Intelligence and Soft
677 Computing. Springer, pp. 702–711.

- 678 Wang, J., Wang, X., 2012. A spatial clustering method for points-with-
679 directions. In: Rough Sets and Knowledge Technology. Springer, pp. 194–
680 199.
- 681 Wing, M. G., Eklund, A., Kellogg, L. D., 2005. Consumer-grade global posi-
682 tioning system (gps) accuracy and reliability. Journal of forestry 103 (4),
683 169–173.
- 684 Yuill, R. S., 1971. The standard deviational ellipse; an updated tool for spa-
685 tial description. Geografiska Annaler. Series B, Human Geography 53 (1),
686 28–39.
- 687 Zhao, G., Wang, T., Ye, J., 2015. Anisotropic clustering on surfaces for crack
688 extraction. Machine Vision and Applications 26 (5), 675–688.
- 689 Zhong, X., Duckham, M., 2016. Characterizing the shapes of noisy, non-
690 uniform, and disconnected point clusters in the plane. Computers, Envi-
691 ronment and Urban Systems 57, 48–58.
- 692 Zhou, W., Xiong, H., Ge, Y., Yu, J., Ozdemir, H. T., Lee, K. C., 2010.
693 Direction clustering for characterizing movement patterns. In: IRI. pp.
694 165–170.

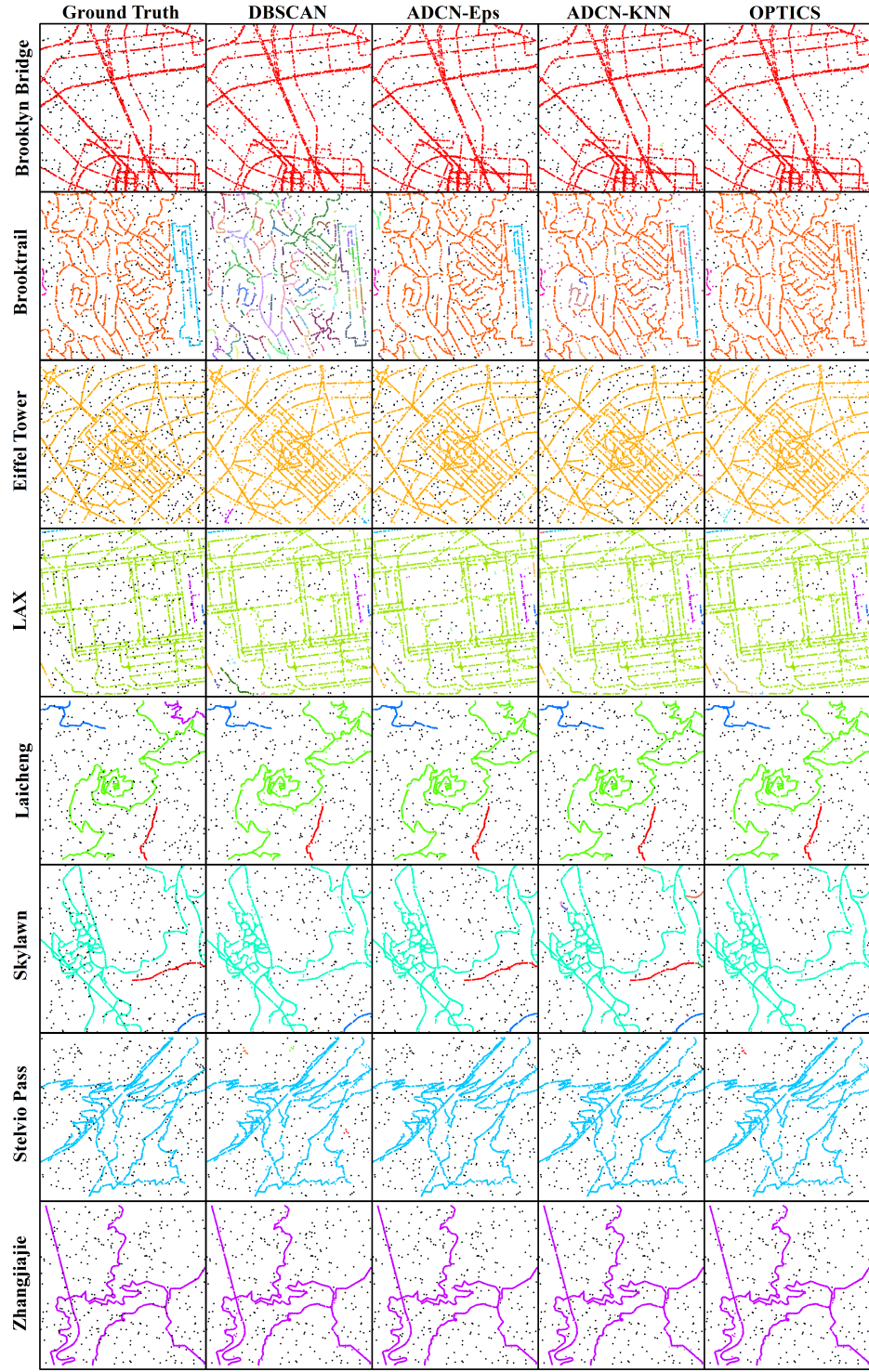


Figure 6: Ground truth and best clustering result comparison for eight real-world cases.

Table 1: Clustering quality comparisons

| Case | Buffer | NMI | | | OPTICS | Rand | | | |
|-----------------|--------|--------|----------|----------|--------|--------|----------|----------|--------|
| | | DBSCAN | ADCN-Eps | ADCN-KNN | | DBSCAN | ADCN-Eps | ADCN-KNN | OPTICS |
| bridge | 0m | 0.937 | 0.957 | 0.957 | 0.937 | 0.985 | 0.991 | 0.992 | 0.985 |
| | 5m | 0.948 | 0.966 | 0.967 | 0.949 | 0.989 | 0.993 | 0.994 | 0.989 |
| | 10m | 0.938 | 0.973 | 0.968 | 0.944 | 0.988 | 0.995 | 0.995 | 0.989 |
| circle | 0m | 0.864 | 0.865 | 0.912 | 0.864 | 0.955 | 0.964 | 0.978 | 0.955 |
| | 5m | 0.859 | 0.897 | 0.916 | 0.859 | 0.955 | 0.974 | 0.978 | 0.955 |
| | 10m | 0.864 | 0.911 | 0.923 | 0.864 | 0.960 | 0.979 | 0.982 | 0.960 |
| circleNarrow | 0m | 0.914 | 0.951 | 0.958 | 0.914 | 0.974 | 0.988 | 0.991 | 0.974 |
| | 5m | 0.939 | 0.946 | 0.965 | 0.939 | 0.983 | 0.987 | 0.993 | 0.983 |
| | 10m | 0.923 | 0.962 | 0.962 | 0.923 | 0.976 | 0.991 | 0.992 | 0.976 |
| circleRoad | 0m | 0.689 | 0.704 | 0.725 | 0.689 | 0.934 | 0.945 | 0.952 | 0.934 |
| | 5m | 0.737 | 0.758 | 0.779 | 0.737 | 0.950 | 0.963 | 0.962 | 0.951 |
| | 10m | 0.730 | 0.778 | 0.821 | 0.730 | 0.946 | 0.963 | 0.971 | 0.946 |
| curve | 0m | 0.918 | 0.946 | 0.955 | 0.918 | 0.978 | 0.989 | 0.991 | 0.978 |
| | 5m | 0.924 | 0.947 | 0.956 | 0.924 | 0.980 | 0.990 | 0.992 | 0.980 |
| | 10m | 0.916 | 0.943 | 0.947 | 0.916 | 0.978 | 0.988 | 0.989 | 0.978 |
| ellipse | 0m | 0.978 | 0.982 | 0.976 | 0.978 | 0.996 | 0.997 | 0.995 | 0.996 |
| | 5m | 0.979 | 0.982 | 0.980 | 0.979 | 0.996 | 0.997 | 0.996 | 0.996 |
| | 10m | 0.975 | 0.980 | 0.978 | 0.974 | 0.996 | 0.997 | 0.996 | 0.996 |
| ellipseWidth | 0m | 0.917 | 0.935 | 0.935 | 0.917 | 0.985 | 0.989 | 0.988 | 0.985 |
| | 5m | 0.919 | 0.933 | 0.939 | 0.919 | 0.988 | 0.989 | 0.989 | 0.988 |
| | 10m | 0.931 | 0.938 | 0.941 | 0.931 | 0.990 | 0.991 | 0.991 | 0.989 |
| multiBridge | 0m | 0.935 | 0.790 | 0.957 | 0.938 | 0.983 | 0.935 | 0.992 | 0.984 |
| | 5m | 0.958 | 0.883 | 0.977 | 0.958 | 0.992 | 0.968 | 0.996 | 0.992 |
| | 10m | 0.964 | 0.830 | 0.985 | 0.964 | 0.994 | 0.947 | 0.998 | 0.994 |
| rectCurve | 0m | 0.886 | 0.893 | 0.907 | 0.886 | 0.963 | 0.969 | 0.973 | 0.963 |
| | 5m | 0.909 | 0.910 | 0.908 | 0.915 | 0.974 | 0.977 | 0.974 | 0.974 |
| | 10m | 0.921 | 0.923 | 0.911 | 0.922 | 0.975 | 0.977 | 0.977 | 0.975 |
| spiral | 0m | 0.740 | 0.756 | 0.774 | 0.740 | 0.913 | 0.930 | 0.938 | 0.913 |
| | 5m | 0.776 | 0.812 | 0.809 | 0.776 | 0.927 | 0.946 | 0.948 | 0.927 |
| | 10m | 0.745 | 0.788 | 0.795 | 0.745 | 0.918 | 0.950 | 0.952 | 0.918 |
| square | 0m | 0.745 | 0.751 | 0.794 | 0.745 | 0.934 | 0.920 | 0.944 | 0.934 |
| | 5m | 0.751 | 0.778 | 0.830 | 0.752 | 0.932 | 0.928 | 0.959 | 0.932 |
| | 10m | 0.744 | 0.716 | 0.801 | 0.743 | 0.935 | 0.893 | 0.944 | 0.935 |
| star | 0m | 0.887 | 0.901 | 0.914 | 0.887 | 0.968 | 0.977 | 0.980 | 0.968 |
| | 5m | 0.903 | 0.899 | 0.916 | 0.900 | 0.974 | 0.977 | 0.982 | 0.974 |
| | 10m | 0.902 | 0.778 | 0.909 | 0.902 | 0.974 | 0.924 | 0.981 | 0.974 |
| Brooklyn Bridge | 0m | 0.378 | 0.542 | 0.490 | 0.378 | 0.888 | 0.930 | 0.925 | 0.888 |
| | 5m | 0.442 | 0.604 | 0.579 | 0.440 | 0.900 | 0.943 | 0.941 | 0.900 |
| | 10m | 0.504 | 0.639 | 0.581 | 0.507 | 0.915 | 0.950 | 0.944 | 0.915 |
| Brooktrail | 0m | 0.441 | 0.431 | 0.421 | 0.440 | 0.742 | 0.765 | 0.756 | 0.742 |
| | 5m | 0.476 | 0.512 | 0.489 | 0.475 | 0.750 | 0.825 | 0.800 | 0.750 |
| | 10m | 0.387 | 0.555 | 0.498 | 0.387 | 0.712 | 0.852 | 0.799 | 0.711 |
| Eiffel Tower | 0m | 0.397 | 0.481 | 0.492 | 0.397 | 0.851 | 0.882 | 0.898 | 0.851 |
| | 5m | 0.459 | 0.566 | 0.571 | 0.459 | 0.868 | 0.906 | 0.921 | 0.868 |
| | 10m | 0.411 | 0.553 | 0.553 | 0.411 | 0.861 | 0.907 | 0.923 | 0.861 |
| LAX | 0m | 0.557 | 0.607 | 0.593 | 0.557 | 0.867 | 0.898 | 0.905 | 0.867 |
| | 5m | 0.591 | 0.667 | 0.584 | 0.591 | 0.883 | 0.921 | 0.903 | 0.883 |
| | 10m | 0.485 | 0.590 | 0.637 | 0.479 | 0.857 | 0.903 | 0.925 | 0.857 |
| Laicheng | 0m | 0.768 | 0.807 | 0.804 | 0.768 | 0.857 | 0.874 | 0.874 | 0.857 |
| | 5m | 0.761 | 0.815 | 0.808 | 0.761 | 0.856 | 0.878 | 0.905 | 0.856 |
| | 10m | 0.773 | 0.823 | 0.809 | 0.773 | 0.861 | 0.880 | 0.911 | 0.861 |
| Skylawn | 0m | 0.618 | 0.822 | 0.733 | 0.618 | 0.871 | 0.956 | 0.927 | 0.871 |
| | 5m | 0.642 | 0.690 | 0.807 | 0.642 | 0.877 | 0.899 | 0.955 | 0.877 |
| | 10m | 0.729 | 0.703 | 0.822 | 0.729 | 0.927 | 0.905 | 0.957 | 0.927 |
| Stelvio Pass | 0m | 0.640 | 0.715 | 0.717 | 0.656 | 0.945 | 0.962 | 0.963 | 0.946 |
| | 5m | 0.739 | 0.791 | 0.768 | 0.739 | 0.962 | 0.974 | 0.975 | 0.962 |
| | 10m | 0.686 | 0.798 | 0.766 | 0.686 | 0.953 | 0.975 | 0.978 | 0.953 |
| Zhangjiajie | 0m | 0.760 | 0.832 | 0.799 | 0.760 | 0.964 | 0.978 | 0.976 | 0.964 |
| | 5m | 0.772 | 0.868 | 0.839 | 0.772 | 0.967 | 0.987 | 0.982 | 0.967 |
| | 10m | 0.835 | 0.911 | 0.873 | 0.835 | 0.978 | 0.991 | 0.990 | 0.978 |

Table 2: The number of cases with maximum NMI/Rand for each clustering algorithm

| # of cases | Max NMI | Max Rand |
|------------|---------|----------|
| DBSCAN | 1 | 0 |
| ADCN-Eps | 25 | 19 |
| ADCN-KNN | 33 | 41 |
| OPTICS | 1 | 0 |

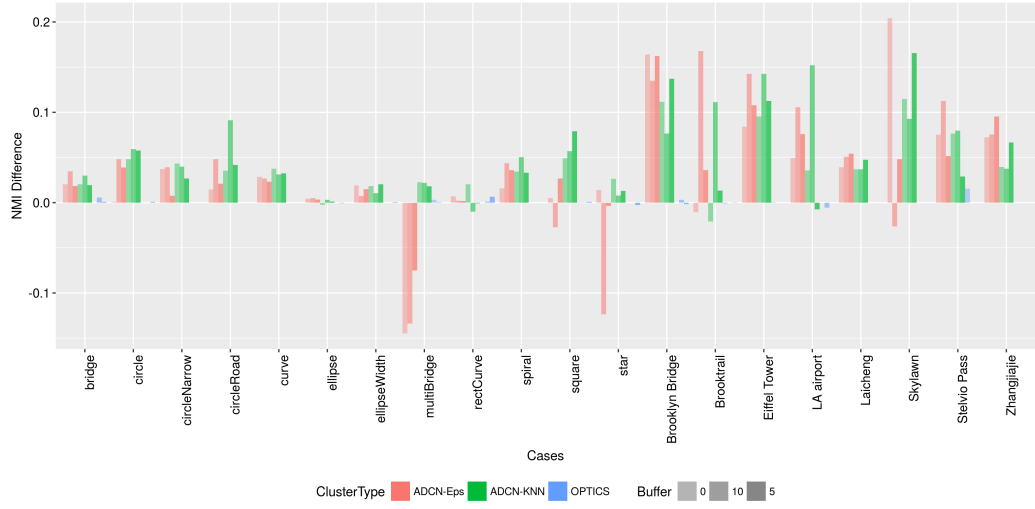


Figure 7: Clustering quality comparisons: NMI Difference between 3 clustering methods and DBSCAN for each case. Synthetic cases are on the left, real-world cases on the right.

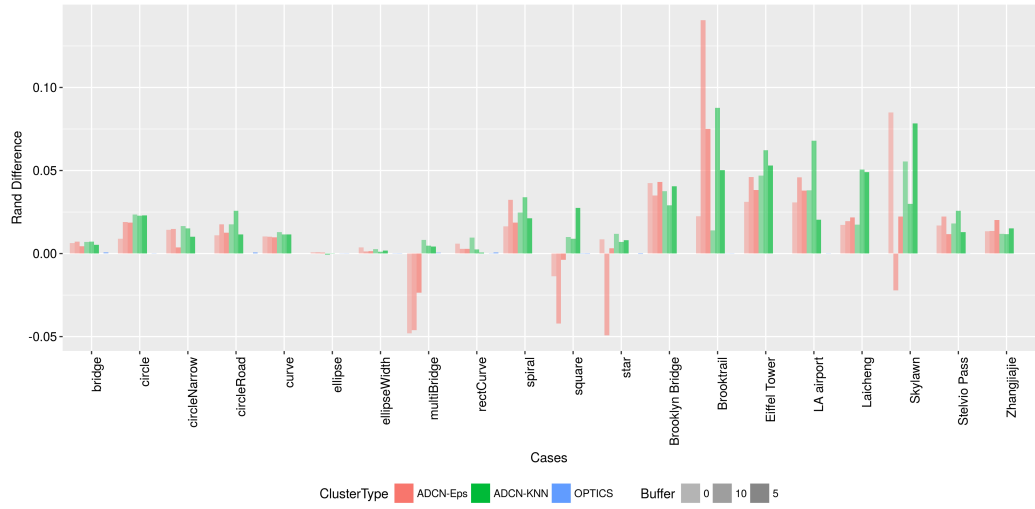


Figure 8: Clustering quality comparisons: Rand Difference between 3 clustering methods and DBSCAN for each case. Synthetic cases are on the left, real-world cases on the right.

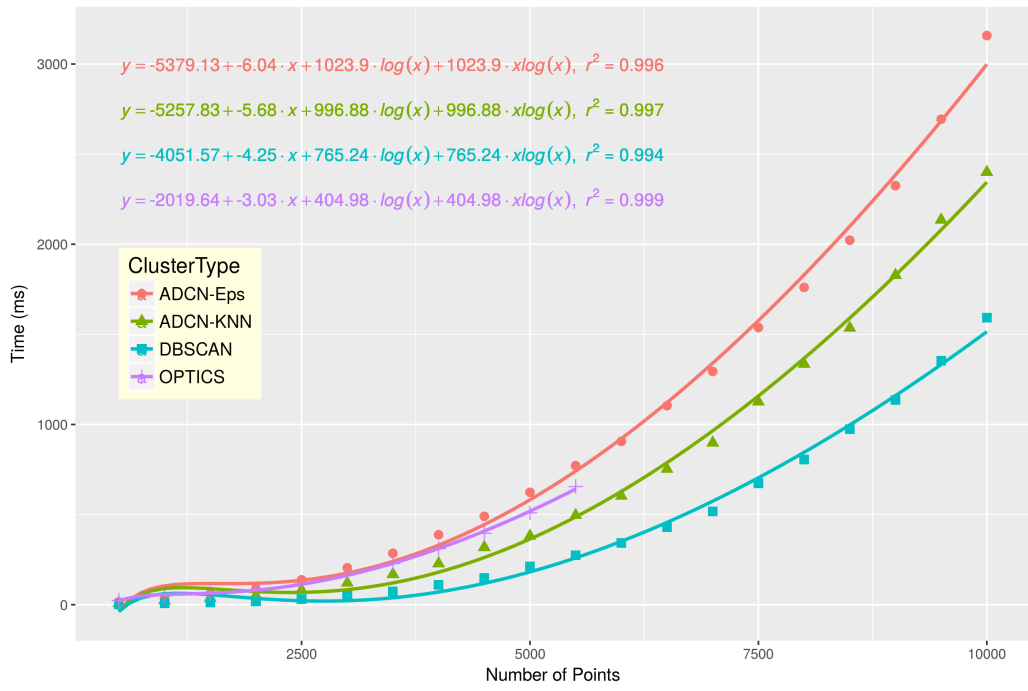


Figure 9: Comparison of clustering efficiency with different dataset sizes; runtimes are given in millisecond (The used OPTICS library failed on datasets exceeding 5500 points)